SANDIA REPORT

SAND2001-1861
Unlimited Release
Printed July 2001

Novel Acoustically Driven Micro-Optoelectronic Devices

Barbara L. Wampler, R. L. White, J. L. Reno, and E. D. Jones

Prepared by
Sandia National Laboratories
Albuquerque, New Mexico 87185 and Livermore, California 94550

Sandia is a multiprogram laboratory operated by Sandia Corporation, a Lockheed Martin Company, for the United States Department of Energy under Contract DE-AC04-94AL85000.

Sandia National Laboratories

Issued by Sandia National Laboratories, operated for the United States Department of Energy by Sandia Corporation.

Available to DOE and DOE contractors from
U.S. Department of Energy
Office of Scientific and Technical Information
P.O. Box 62
Oak Ridge, TN 37831

Telephone: (865)576-8401
Facsimile: (865)576-5728
E-Mail: reports@adonis.osti.gov
Online ordering: http://www.doe.gov/bridge

Available to the public from
U.S. Department of Commerce
National Technical Information Service
5285 Port Royal Rd
Springfield, VA 22161

Telephone: (800)553-6847
Facsimile: (703)605-6900
E-Mail: orders@ntis.fedworld.gov
Online order: http://www.ntis.gov/ordering.htm

SAND2001-1861
Unlimited Release
Printed July 2001

Novel Acoustically Driven Micro-Optoelectronic Devices

Barbara L. Wampler
Microsensors Research

R.L. White, J.L. Reno, and E.D. Jones
Semiconductor Materials and Device Sciences Department

Sandia National Laboratories
P. O. Box 5800
Albuquerque, NM 87185-0601

Abstract

This report represents the completion of a two-year Laboratory-Directed Research and Development program that focused on research for a novel approach for combining optical and surface acoustic wave techniques. The basis for this work is the spatial movement of laser-generated excitons by a surface acoustic wave in a GaAs/$Al_{0.30}Ga_{0.70}As$ 8-nm wide quantum well at liquid helium temperature. When surface acoustic waves are applied to laser-generated excitons, the number of photons emitted from the illuminated region decreases with larger applied RF voltages and longer pulse widths, demonstrating that laser-generated excitons are transported away from their point of origin by the surface acoustic waves. Three separate objectives of this research were to (1) show the generation of excitons in a GaAs/AlGaAs quantum well structure; (2) fabricate the surface acoustic waves devices on the GaAs/AlGaAs quantum well structure and show that the surface acoustic waves can be generated; and (3) investigate the interaction of the excitons and the surface acoustic waves. These studies include the description of the experimental methods, sample design and fabrication, and cryogenic testing necessary to accomplish these objectives. Details of the photolithography of the surface-acoustic-wave pattern is also presented. Finally, exciton photon count rates versus surface acoustic wave input voltage will be shown for different pulse widths clearly demonstrating exciton movement by surface acoustic waves.

Key Words: Semiconductors, GaAs, AlGaAs, surface acoustic waves, exciton.

Acknowledgements

This research was supported by Sandia National Laboratories, a multiprogram laboratory operated by Sandia Corporation, a Lockheed Martin Company, for the United States Department of Energy under contract DE-AC04-94L85000.

Contents

This Page Intentionally Left Blank

1. Introduction

This project investigates a novel approach for combining optical and surface acoustic wave (SAW) techniques. The basis for this study is the spatial movement of laser-generated electron-hole pairs, also called excitons, by a surface acoustic wave. This report will detail the design and photolithographic fabrication of surface acoustic wave devices on a gallium arsenide/aluminum gallium arsenide quantum well structure. It will also describe the testing of these surface acoustic wave devices at liquid helium temperature and demonstrate that laser-generated excitons are transported when surface acoustic waves are applied.

1.1. Background

Previous work has shown that the piezoelectric fields of a SAW can effectively couple to quasi-two-dimensional mobile carriers in a semiconductor.[1] The strong lateral piezoelectric fields accompanying a surface acoustic wave on a semiconductor quantum well structure will field-ionize and dissociate optically generated excitons and efficiently trap the created electron-hole pairs in the moving lateral potential superlattice of the sound wave. The resulting spatial separation of the photogenerated ambipolar charges leads to an increase of the radiative lifetime by orders of magnitude as compared to the unperturbed excitons. The confinement of the photogenerated electron-hole pairs to two dimensions, together with the moving lateral superlattice, allows reversible charge separation.[2-4] The strongly reduced wave function overlap results in very long storage times for this polarization that propagates across the sample at the speed of sound. External and deliberate screening of the piezoelectric fields triggers radiative recombination after long delay times at a location on the sample being different from the one of optical excitation.[5,6]

This research was undertaken to report on the interactions between surface acoustic waves and excitons in the two-dimensional electron gas system of the $GaAs/Al_{0.3}Ga_{0.7}As$ heterojunction at liquid helium temperature. This work was aimed at reproducing the findings of Wixforth[1,5,6] and Rocke[3,4], which is to show that when surface acoustic waves are applied to laser-generated excitons, fewer photons are emitted in the illuminated region, and that the photon count decreases with larger voltages and longer pulse widths. Repro-

duction of the previous research will show proof-of-concept which can then be used to define future research directions.

1.2. Surface acoustic waves

Surface acoustic waves (SAWs) are elliptically polarized waves that are a combination of a longitudinal (compressional) wave as well as a transverse (shear) wave coupled together in a fixed ratio. In piezoelectric substrates there is also an accompanying electrostatic wave. The crystalline structure of a piezoelectric substrate is acentric. When a mechanical stress is applied to a piezoelectric material, ions are displaced in an asymmetric manner and electric dipoles are produced in the crystal. This generates a polarization change or voltage. Conversely, when an electric field is applied, dipoles are induced in the crystal and the resulting small atomic displacements produce a mechanical strain. If an alternating field is applied to a piezoelectric crystal, the electric displacement also varies periodically. Surface waves propagate along the surface of the piezoelectric substrate, and the amplitude of the wave motion into the depth of the substrate decays within a distance on the order of a wavelength λ. See Figure 1 for details. For a 200 MHz SAW device on GaAs, the wavelength is approximately 14 μm. The wave is not uniform in the y-direction. Over the size of the samples used here, no variation is seen in the transverse direction, or

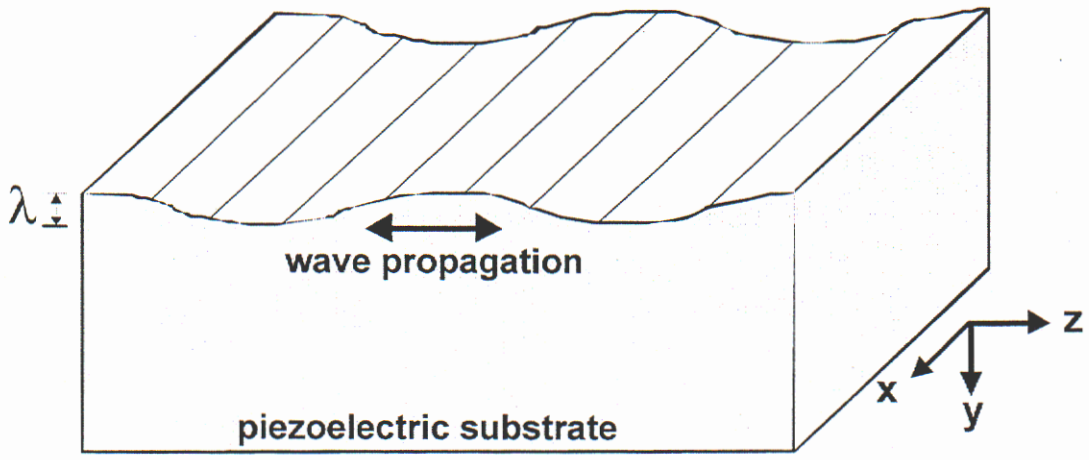

Figure 1: Surface waves propagate along the substrate in the z-direction and decay into the depth of the substrate (y-direction) within a distance on the order of a wavelength λ. No variation is seen in the x-direction.

x-direction, along the surface. Particles move both in the direction of wave propagation, the z-direction, and perpendicular to the surface, the y-direction.

The interdigital transducer (IDT) is the most important component in the SAW device and is illustrated in Fig. 2. It is used to interface between the electrical circuit and the acoustic delay line both as a transmitter (electrical to acoustic) and as a receiver (acoustic to electric). The IDT converts the electrical signal to an acoustic signal. An IDT consists of a metallic pattern of interdigitated electrodes fabricated on the top polished surface of the piezoelectric substrate using photolithographic techniques. A complete delay line consists of two IDTs, one acting as a transmitter and the other as a receiver.

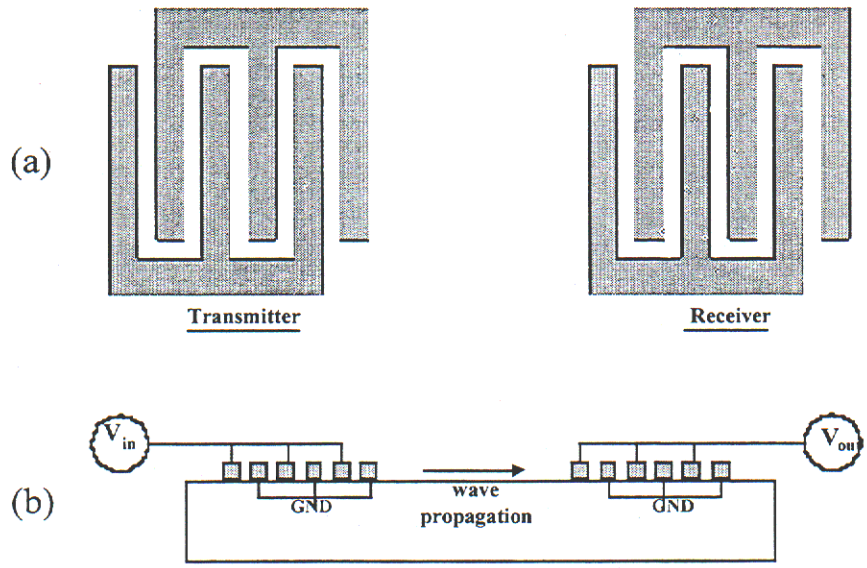

Figure 2: (a) The IDT as a transmitter and a receiver. (b) A SAW device, showing the IDTs as well as wave propagation

Metallic IDTs are deposited in a vacuum on a piezoelectric substrate such as quartz or gallium arsenide. For the most efficient transducer operation, the SAW wavelength λ should match the IDT periodicity. This occurs when the fingers are spaced at half-wavelength intervals, where the wavelength $\lambda = v/f$. Here v is the surface wave velocity and f is the excitation frequency. When an alternating voltage of frequency f is applied to the IDT, an electric field is created between adjacent fingers. A strain field is also generated because of the electromechanical interaction in the piezoelectric substrate. This strain field is an imprint of the IDT and propagates away from the IDT in both directions as a surface wave. The surface wave is then detected by a second IDT as the SAW passes through it because

the surface wave carries with it an electric field via the piezoelectric effect which generates a voltage between adjacent IDT fingers. For a more extensive review of IDTs, the reader is directed to White.[7]

The substrate material used for the fabrication of the SAW devices for this experiment was gallium arsenide. Gallium arsenide is piezoelectric, but judged it by its capabilities of sustaining a surface acoustic wave (see Ash and Paige[8]), it does not appear to be as attractive a substrate material as quartz. Its piezoelectric coupling is slightly less than quartz and its attenuation slightly higher. However, gallium arsenide is semiconducting which allows the generation of excitons, and it is lattice-matched to aluminum arsenide which allows the growth of a quantum well layer in which to trap the free electron-hole pairs. Also, being semiconducting allows the integration of SAW devices with electronics, if desired, for future research directions.

1.3. Excitons

An exciton is a quantum of electronic excitation energy travelling in a periodic structure, whose motion is characterized by a wave vector. The exciton consists of an electron and a hole coupled together, and it carries no electric charge and cannot contribute to electric conduction. The exciton is represented by the two particles coupled by a Coulomb force. Excitons are the excited electronic energy states of semiconducting and insulating crystals. Such crystals are characterized by the fact that all the excited states are separated from the ground state by a finite (and often large) energy gap. Since in only a few crystals is this energy gap small enough to allow appreciable population of the excited states at normal working temperatures, these states are normally studied by excitation with light. Crystals with an energy gap are transparent for light up to frequencies where $h\nu \sim E_G$, beyond which they begin to absorb. In this equation, h is Planck's constant, ν is the frequency of light, and E_G is the semiconductor bandgap energy. There is also absorption at low infrared frequencies due to lattice vibration and not electronic transitions, but this will not be of concern here. For a more thorough review of excitons, the reader is referred to Dexter and Knox[9] and Kuper and Whitfield.[10]

When a photon is absorbed by a direct bandgap semiconductor, an exciton is generated in the illuminated region. If there are no interactions that perturb the exciton, it will

recombine and emit a photon whose energy is equal to the semiconductor bandgap energy minus the binding energy of the exciton. The presence of a short-pulse duration surface acoustic wave can transport the exciton from its region of origin to another spatial location where the photon can then be emitted. On a piezoelectric substrate, the elliptically polarized surface acoustic waves are accompanied by both lateral and vertical piezoelectric fields, propagating at the speed of sound. These fields field ionize optically generated excitons and confine the resulting electrons and holes in the moving lateral potential wells separated by one-half wavelength of the surface acoustic wave.[5] See Figure 3. Excitons, although neutral entities, are moved by the electric field generated by the surface acoustic wave. The actual mechanism for the movement of the excitons is via the separation of the excitons into electron-hole pairs which are affected by the electric field gradient.[4] Because of this SAW-induced separation, the electron-hole recombination probability is dramatically reduced, and the radiative lifetime is increased when compared to the unperturbed

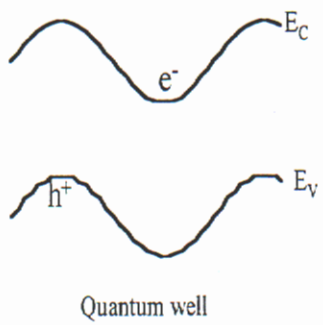

Figure 3: Exciton transport mechanism, showing the ionized exciton confined by the surface acoustic wave. The electron is trapped in the potential minima of the conduction band, and the hole is trapped in the maxima of the valence band

case (~ 1 nsec). The dynamically trapped electron-hole pairs can be physically transported over microscopic distances at the speed of sound, and they will emit photons upon coming to rest at the new position.

1.4. Quantum wells

Different semiconductor materials have different energy bandgaps. The energy bandgap is defined as the energy difference between the valence band and the conduction band. The valence band is the energy band in which the electrons occupy bonding orbitals and are not generally free to move in response to an electric field. The conduction band is the energy band in which the electrons are free to move under the application of an electric field. If two materials of different bandgaps are grown on top of one another, a discontinu-

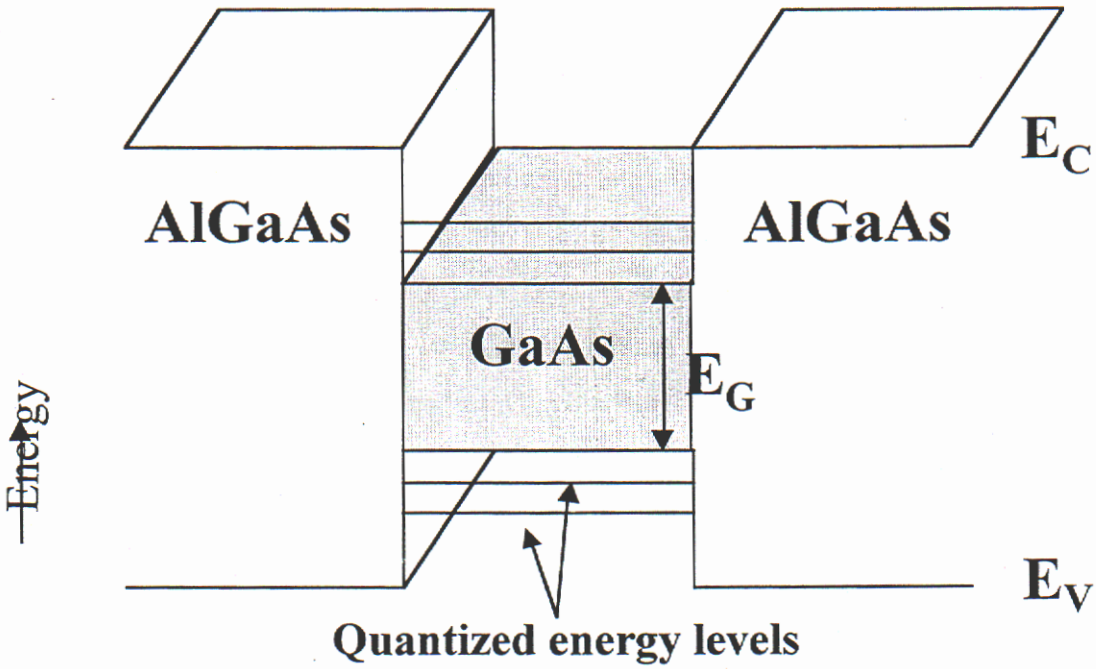

Figure 4: Single quantum well formed by GaAs/AlGaAs, showing the quantized energy levels

ity in the conduction and the valence bands occurs at the interface between the two materials, due to the discontinuity in the energy gap. Depending on how much of the discontinuity occurs within the conduction band or the valence band, a discontinuity in the electric potential at the interface can be formed. If a material of smaller bandgap is sandwiched between two layers of material of larger bandgap, a finite potential well is formed. See Figure 4. This is the case for this research, where gallium arsenide is layered between aluminum gallium arsenide, a material with which it is lattice-matched. If the width of the well is made sufficiently small that spatial quantization effects occur in the direction perpendicular to the interface, then the well is said to be a single quantum well. As a result, electrons confined within the well can have only discrete quantized energies in specific directions. In the directions parallel to the interface the electronic energies are not quantized and the electrons retain their band properties. The electrons have one fewer spatial

degree of freedom when confined to the potential well formed at the interface. This resulting system is called a two-dimensional electron gas.

1.5. Purpose of this work

The purpose of this study is to implement the instrumentation and fabricate the SAW devices to demonstrate the movement of excitons using surface acoustic waves to reproduce the previous research on this topic. Three separate objectives of this study are to (1) show the generation of excitons in a GaAs/AlGaAs quantum well structure; (2) fabricate the SAW devices on the GaAs/AlGaAs quantum well structure and show that the surface acoustic waves can be generated; and (3) investigate the interaction of the excitons and the surface acoustic waves. A laser will illuminate the area between SAW transducers patterned on a GaAs/AlGaAs quantum well structure, and the photon output will be shown to decrease when the surface acoustic waves are initiated on the substrate. The experimental methods, sample design and fabrication, and cryogenic testing necessary to accomplish these objectives will be described.

Section 2 describes the experimental details of this report. The sample design and growth will be discussed. The photolithography of the SAW pattern will be given, starting with the mask generation. Diagrams and descriptions of the optical detection system used to detect the exciton transport will be given. Section 3 contains the results and discussion from the experiments. The photoluminescence spectra for the GaAs/AlGaAs sample will be shown. The SAW device network analysis will be discussed. Plots of the photon counts versus SAW input voltage will be shown for different pulse widths. Section 4 details the conclusions and future directions to be taken for this experiment.

2. Experimental Details

2.1. GaAs sample design and growth

The undoped quantum well samples were grown by molecular beam epitaxy on a 3" undoped (100) semi-insulating GaAs substrate which was 625 μm thick. The epitaxy consists of 300 nm of undoped GaAs grown on the substrate to act as an ultra-pure base for the subsequent layers. This was followed by a 100 nm $Al_{0.3}Ga_{0.7}As$ barrier layer. The quantum well consists of 8 nm of GaAs grown on top of this barrier layer. The quantum well layer is then covered by another 100 nm $Al_{0.3}Ga_{0.7}As$ barrier layer, which is followed by a 10 nm GaAs cap layer. The capping layer is necessary because the AlGaAs layer oxidizes easily. See Figure 5. The crystal cut used here (the (100) surface with [110] propagation) results in the highest achievable electromechanical coupling coefficient for surface acoustic waves on gallium arsenide.[8]

For this experiment, the quantum well is to be used as the trapping location for the spatially separated electron-hole pairs. As described in Section 1.4, the quantum well has discrete energy levels, and this is where the electron-hole pairs will reside while they are being transported by the surface acoustic wave.

Bulk GaAs was not used for this experiment because excitons are harder to generate and less confined in the bulk material. Electrons and holes in the GaAs quantum well are confined to two dimensions and are more likely to form an exciton. In the bulk material,

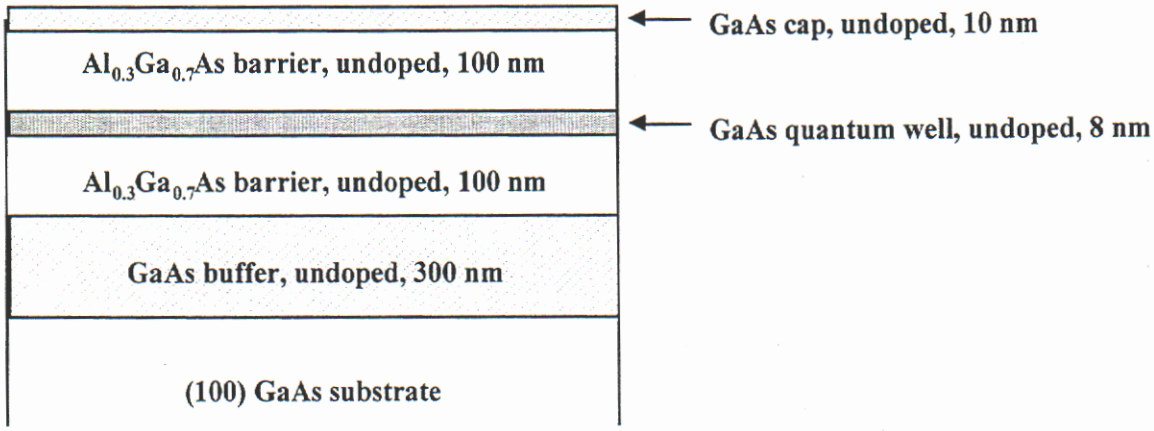

Figure 5: A cross-section of the MBE growth layers for the GaAs/AlGaAs quantum well structure grown for this research.

the electrons and holes have three dimensions in which to travel, and the probability of combination is much less. Also, bulk GaAs has nonradiative surface states while the GaAs quantum well is isolated from the surface so surface states are removed. The exciton binding energy in GaAs/AlGaAs quantum wells is also larger than the bulk value, 12 meV versus 4 meV, respectively. A larger binding energy gives rise to a smaller Bohr radius for the quantum well exciton, and hence a larger oscillator strength for the optical transition.

The photoluminescence spectra from the GaAs quantum well is uniquely identifiable from the spectra for the GaAs cap and the epitaxially grown GaAs layers. The photons emitted from the quantum well are at an energy which is the bandgap energy plus the increase in the energy due to quantum well confinement minus the exciton binding energy in the quantum well. The photons emitted from the GaAs cap and the epitaxially grown GaAs are at the bandgap energy minus the bulk (3-D) exciton binding energy. Because of two-dimensional confinement effects, the exciton binding energy in the quantum well is larger (as much as a factor of four) than the bulk GaAs exciton binding energy of 4 meV. Thus, the emitted photons from a 100-Å-wide GaAs quantum well are at higher energies (shorter wavelengths) compared to those emitted from either the GaAs cap layer or the GaAs substrate.

2.2. SAW design

Surface acoustic waves are modes of elastic energy propagating along the surface of an elastic medium. The displacement amplitudes essentially decay in an exponential fashion into the bulk of the substrate. The main energy flow is concentrated within a distance of the order of a wavelength λ beneath the surface. The particle displacement at and beneath the surface is elliptic, leading to an elliptical polarization of the wave. The SAW velocity for (100) GaAs and [110] propagation is v = 2865 m/sec,[8] and the interdigitated transducers for this project were designed to operate at a center frequency of 200 MHz. For these conditions, the theoretical SAW wavelength should be 14.3 μm.

The interdigital transducer is the most important component in the SAW device. Each transducer finger is a discrete source for the generation of surface waves in the piezoelectric medium because the piezoelectrically generated stress varies with position near

each transducer finger. A simple transfer function relates the continuous wave voltage V applied to a finger and electrical potential F associated with the waves radiated in each direction[11] gives

$$\Phi^{\pm} = \mu_s V \ , \tag{1}$$

where μ_s is a substrate-dependent constant, $\Phi+$ is associated with the rightward propagating SAW, and Φ^- is a leftward propagating SAW. The parameter μ_s may be considered to be frequency independent. The frequency response arises mainly from the interference between finger contributions. When an array of fingers is excited, as occurs in an interdigital transducer, the wave potential for a rightward propagating wave Φ^+ evaluated at position z is a vector sum of the contributions of each finger[12] or

$$\Phi^{+}(z) = \mu_s \sum_{n=0}^{N-1} V_n \, e^{jk(z-z_n)} \ , \tag{2}$$

where z_n is the position of the n^{th} finger excited with voltage V_n, $k = 2\pi/\lambda$, and N is the total number of fingers. This equation has the form of a discrete Fourier transform of the sequence V_n. The frequency response of the device is proportional to the Fourier transform of the sequence of transducer finger contributions. Desired frequency response can be achieved by varying the individual finger contributions. If N identical fingers are spaced periodically with period d and excited with alternating voltages $V_n = (-1)^n V_0$, Equation 2 becomes[12]

$$\Phi^{+}(0) = \mu_s V_0 \sum_{n=0}^{N-1} (-1)^n \, e^{-jnkd/2} \ . \tag{3}$$

The sum in Equation 3 is a geometric series whose elements become unity, and add constructively, when $kd/2 = m\pi$, *or* $\lambda = d/m$, where m is an odd integer. This condition defines

the relationship between SAW wavelength, λ, and the transducer periodicity, d. The IDT excites odd harmonics at odd multiples of the synchronous frequency, i.e., $f_m = mf_0$.

When moving away from the synchronous frequency, the addition of components from individual fingers becomes incoherent, thus giving rise to the frequency response[12]

$$\left|\Phi^{+}(f)\right| = \left|\frac{\sin(X)}{X}\right|, \tag{4}$$

in which

$$X = \frac{N_p \pi (f - f_0)}{f_0}, \tag{5}$$

where f_0 is the transducer's synchronous frequency and N_p is the number of IDT periods: $N_p = N/2$. See Figure 6. Note that when X is a multiple of p, Φ^{+} is zero as a result of the complete cancellation between finger contributions. Consequently, the quality factor B

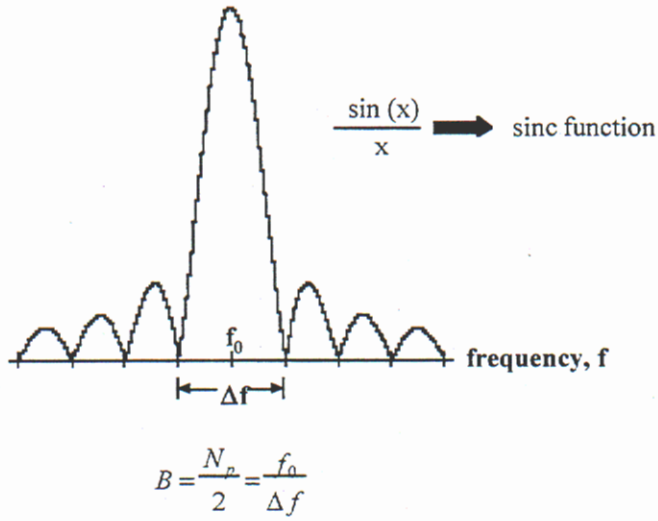

Figure 6: A plot of |*sin (x)/x*|, which is the theoretical SAW device network analysis. The signal is centered around the center frequency, f_0, with a bandwidth of Δf. The quality factor B is dictated by the number of finger-pairs used.

between first nulls on either side of the synchronous frequency is[12]

$$B = \frac{N_p}{2} = \frac{f_0}{\Delta f}\ , \tag{6}$$

where Δf is the bandwidth. Thus, B is directly proportional to the number of IDT fingers.

The IDTs for this experiment consisted of forty finger-pairs with a period of 14 mm. Each finger was 3.5 μm wide with a 3.5 μm wide spacing between. The length of each finger was 233 μm with a 7 μm spacing between the end of the finger and the opposite finger-set. The distance between the transmitting and receiving transducers was 1865 μm. The bandwidth for this configuration is 10 MHz. See Figure 7 for a figure of the IDT dimensions

2.3 Mask design

The software DW-2000, version 7.0 from Design Works was used to design the mask layouts used for the SAW device photolithography. Photronics, Inc. of Colorado Springs, CO manufactured the 4" chrome plates. The design entailed an array of SAW devices on the mask with alignment marks necessary for multilevel photolithography. The array of SAW devices were laid out in a 3" square to maximize the number of devices that could be fabricated on the 3" diameter substrate. The dimensions used were those found in Figure 7.

Previous testing of SAW devices on GaAs quantum well structures similar to those used for this experiment showed capacitive coupling to the two-dimensional electron gas underneath the SAW devices. It was decided that if the quantum well were removed underneath the transducers, the coupling could be avoided.[1] A mask was made to allow an etch of the quantum well only underneath each of the IDTs, leaving the quantum well intact in the acoustic wave path between the transducers. This etch would be done prior to the SAW device lithography. See Figure 8. The etched areas were designed to completely encompass each transducer so that the metallization of the SAW device would be planar.

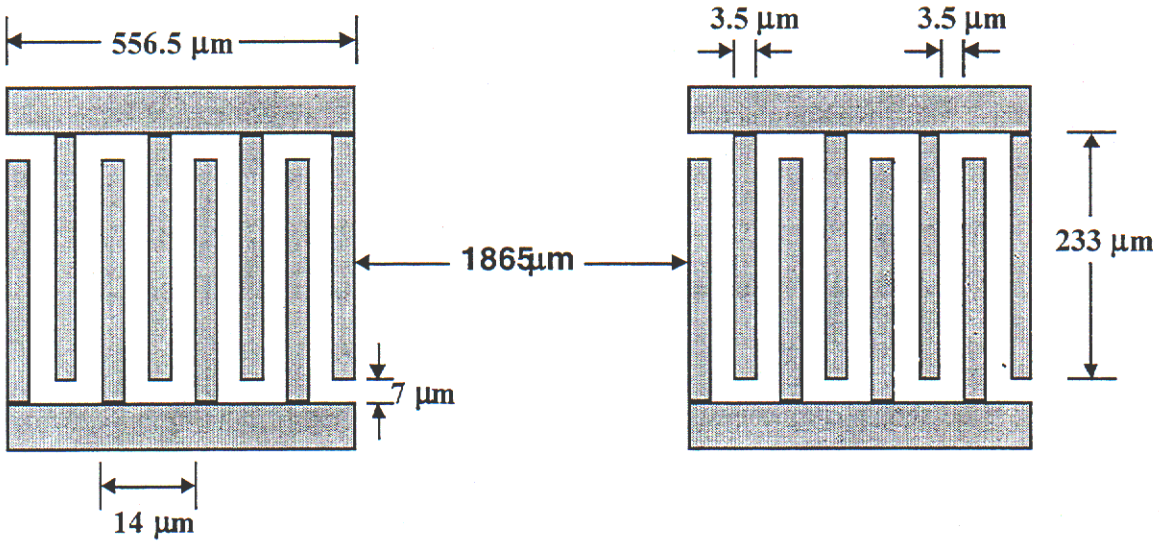

Figure 7: An overview of the IDT dimensions used for the SAW device design

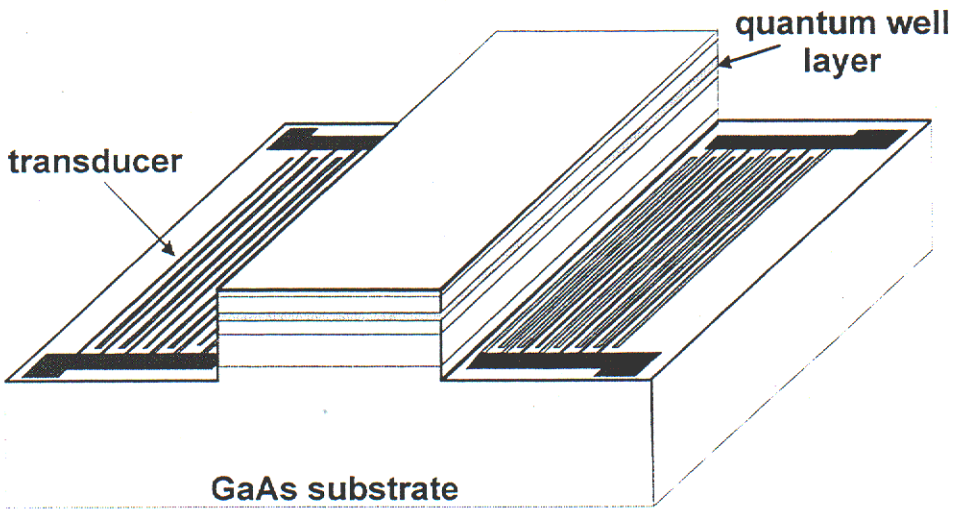

Figure 8: A cross-section of the SAW device with the quantum well etch. The quantum well is left intact in the acoustic wave path between transducers. The etch can be seen to extend through the layers grown by MBE, down to the GaAs substrate

This etched area allowed for at least 40 μm on any side of the SAW device to ensure that alignment was not a concern.

For the best resolution of the mask features using contact photolithography, the substrate and mask must be in contact as close as possible. However, to nullify the effect of the quantum well and avoid the capacitive coupling, the 518 nm deposited by MBE would need to be etched, down to the (100) GaAs substrate. This etch step of approximately 0.5 mm, though, would still allow for very good resolution using contact lithography.

2.4 Lithography

The surface acoustic wave devices were fabricated in the Compound Semiconductor Research Laboratory at Sandia National Laboratories, which is a class 100 clean room. The 3" GaAs quantum well wafer was scribed and broken into three pieces. This was to allow for any subsequent design changes which might be necessary for this experiment. Approximately one-third of the wafer was used to fabricate this first batch of SAW devices. A blank GaAs wafer, which did not have a quantum well, was also scribed and broken. A piece of this wafer was to act as a calibration for the etch process.

A critical parameter when fabricating SAW devices on a piezoelectric medium is that the wave propagation must be optimized to achieve the minimum loss between transducers. For (100) gallium arsenide, this is achieved by assuring that the wave propagation between transducers is along the [110] crystal direction, which is parallel to the major flat. At each lithography step, special attention was paid to this fact and the features on the mask were first aligned to the major flat on the wafer.

The first process for the two wafer pieces was to photolithographically pattern the etch mask onto the wafers before using a reactive-ion etch process to dry etch the material. The two wafer pieces were subjected to a solvent clean which consisted of a five minute rinse in acetone, followed by a methanol spray, then a five minute rinse in isopropanol. A five minute deionized water rinse was used to remove any remaining solvent residue. The wafers were then sprayed with a solution of ammonium hydroxide diluted with deionized water in a ratio of 1:20 to remove the native oxide that is on the wafer surface and increase

the adhesion of the next processing step. Immediately after this rinse, the wafers were placed in an automated vacuum oven, the YES Model 58SM HMDS Vapor Prime Oven, which dispenses hexamethyldisilizane onto the wafers to promote adhesion between the wafer surface and photoresist. AZ9245 photoresist was then spun onto the wafers at 4000 rpm for 30 seconds using a Headway Model PWM101 spinner. Under these conditions, the AZ9245 photoresist is nominally 4.8 μm thick. The photoresist was baked on a hotplate at 110°C for two minutes to remove volatile organic compounds and harden the photoresist. The etch pattern was photolithographically printed onto the wafer using a Karl Suss MA6 aligner, which exposed the photoresist for 15 seconds using hard contact mode. The photoresist was developed in AZ400K 1:4 developer for 190 seconds, resulting in open areas on the wafer where the etch would take place. An LFE barrel asher was used at a power of five watts for five minutes to remove any residual photoresist in the open areas.

The dry etching of the wafers was done in a Semigroup reactive-ion etching system using chlorine and boron trichloride gases. The piece with no quantum well was etched first to ascertain an etch rate for the system, which was initially guessed to be approximately 500 Å per minute. Because the etch needed to be at least through 5180 Å down to the GaAs substrate, a fifteen minute etch was done to allow for variability in the etch rate. The etch depth was checked on an Alpha-Step Model 500 profilometer after the photoresist was removed with acetone. The depth was found on average to be 1.8 μm, with the etch at the center of the wafer being shallower than the edges. The piece containing the GaAs quantum well was then etched for ten minutes, with its etch depth found using the same methods to be on average 1.3 μm. This etch depth is definitely through the quantum well layer and into the GaAs substrate, as was necessary.

The next step in the processing was to pattern the SAW devices onto the wafers. The wafers were again subjected to the solvent clean using acetone, methanol, and isopropanol. The deionized water rinse was followed by the 1:20 ammonium hydroxide in water rinse to remove the oxide. Immediately following this rinse, the wafers were put into the HMDS oven. AZ4110 photoresist was spun on the wafers at 5000 rpm for thirty seconds, and the photoresist was baked on a hotplate at 110°C for ninety seconds. AZ4110 spun

under these conditions is nominally 1.0 μm thick. Using the Karl Suss MA6 aligner, an edgebead exposure was done to remove the thicker photoresist that piles up at the edges of the wafer during spinning. An edgebead mask is the same shape as the wafer, but slightly smaller in size to expose only a thin region of the wafer at the edges. Removing the thicker photoresist at the wafer edge allows for better contact with the mask and is needed especially when trying to pattern features that are less than 5 μm. The edgebead was exposed for 45 seconds under vacuum contact, and it was developed for ninety seconds in Shipley MIF312 developer diluted 1:1.4 in deionized water. The wafer was now placed in the aligner with the SAW device mask. Alignment of the SAW devices with the etched areas on the wafer was accomplished via a global alignment mark positioned at the center of the mask and several smaller alignment marks positioned at several spots around the mask. The initial etch mask had corresponding alignment marks designed into it. After alignment, the SAW device mask was exposed for four seconds using vacuum contact. Shipley MIF312 developer diluted 1:1.4 was used for 150 seconds, resulting in open areas where the SAW device metal will be. The barrel asher was again used at a power of five watts for five minutes to remove residual photoresist in the open areas on the wafer.

Metallization of the SAW devices was achieved using a CVC e-beam evaporator. The samples were rinsed with the 1:20 ammonium hydroxide/deionized water solution to remove the oxide before placing them in the evaporator. The base pressure at the beginning of the evaporation was 5×10^{-7} torr. The metallization consisted of 150 Å of Ti followed by 1500 Å of Au. The samples were then placed in acetone to lift off the metal everywhere the photoresist had not been previously exposed, developed and rinsed away. See Figure 9 for a photo of a SAW device transducer, including the etch.

The resulting SAW devices matched the design specifications with the transducers' fingers and spacings approximately equal at 3.5 μm. Alignment of the SAW device layer to the etch layer was somewhat difficult due to small alignment mark size, but the final result was that the alignment of the SAW devices was parallel to the etch layer but displaced by a few microns in both the x- and y-directions, which was acceptable. As described before, at least forty microns of extra etch had been designed around the SAW

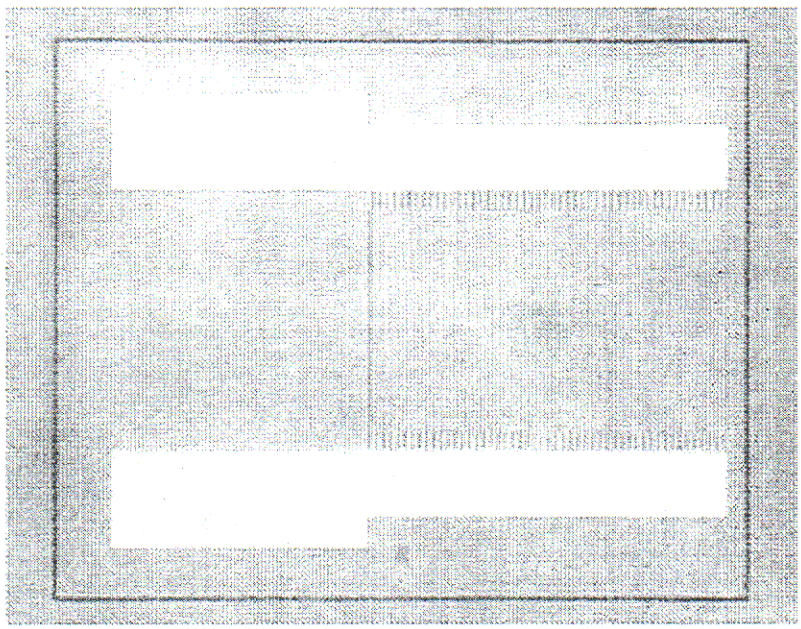

Figure 9: A microscope photograph of a photolithographically fabricated SAW device transducer. The dark line seen to encompass and parallel the transducer on all four sides is the etch which extends down to the GaAs substrate.

device to allow for some misalignment. Because the SAW devices were parallel to the etch layer which had been aligned to the major flat of the wafer, the efficiency of the signal coupling between transducers should be at a maximum.

The SAW devices were diced using an Assembly Technologies dicing saw, Model 1500, with an S1635 blade with a 1.5 mil kerf. This blade was used to minimize the substrate loss during dicing. The SAW devices were glued into a stainless steel flatpack using a two-component epoxy. A Westbond ultrasonic wire bonder was used to make electrical contact between the SAW device and the flatpack.

2.5. Optical detection

The configuration of the light guiding system used for this research is shown in Figure 10. The laser used is a Spectra-Physics Model 2030 argon-krypton ion laser at a wavelength of 514.5 nm. The laser beam energy is coupled into the optical fiber by means of a microscope objective. The same fiber is used to transmit the laser light to the SAW device and to return the luminescence signal, which is directed to the spectrometer and photon counter by a beam splitter and optical elements. The quartz plate beam splitter transmits

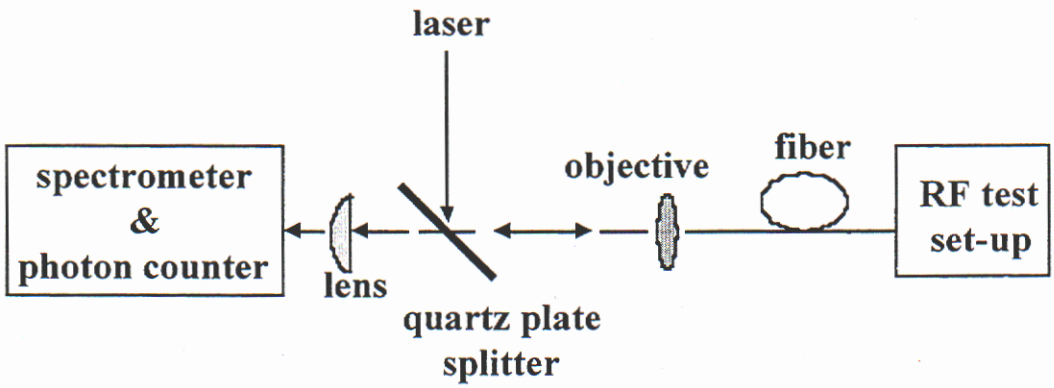

Figure 10: The light guiding system used.

96% of the laser light to the spectrometer and photon counter, while reflecting 4% to the RF test set-up.

Two different types of optical fiber were used for this experiment. The optical fiber from the optics to the liquid helium dewar was a Chromatic Technologies, Inc. 500 Series 100μm/140μm optical fiber cable. The fiber used inside the dewar was an ITT optical fiber waveguide, type T1301 100μm/140μm with a graded index. This fiber is enclosed by a plastic sheath. The difference between the two cables is that the Chromatic Technologies cable is a sturdy commercially made cable while the ITT cable has less jacketing and was more suited to the mounting fixture dimensions.

The mounting fixture for the SAW device is shown in Figure 11. The RF test fixture was machined from a rod of G10 phenolic plastic, which is a high pressure, thermosetting industrial laminated plastic. This material has a lower heat capacity than stainless steel which allows for less boil-off of liquid helium during cryogenic testing. The G10 phenolic plastic has high flexural, impact, and bond strength at room temperature, as well as good electrical properties under dry and humid conditions. The flatpack was attached to the mounting fixture using screws, a brass bar, and a copper plate. The copper plate was placed under the flatpack to act as a ground plane. The brass bar was screwed down onto

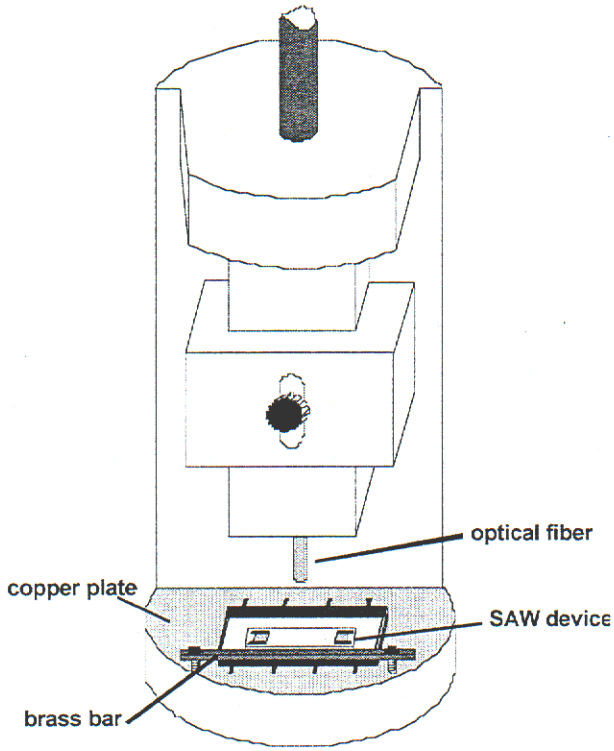

Figure 11: The RF test fixture used for the cryogenic testing of the SAW device.

the edge of the flatpack to make a compression fit between the flatpack and the underlying copper plate. Electrical connection to the flatpack was made using flexible coaxial cable.

The ITT optical fiber was fed down to the SAW device through a hole machined in the fixture. The optical fiber was positioned to be at a point approximately equidistant from both transducers. At room temperature the height of the fiber was adjusted until the SAW device response was attenuated slightly by the fiber touching the SAW device surface. The closer the fiber could be to the SAW device, the better the coupling of the photons back into the fiber, but the surface acoustic wave was detrimentally affected by anything in contact with the substrate surface. The fiber was placed as close to the substrate as possible without contacting the substrate.

2.6 Experimental test set-up

The low-temperature optical-system configuration for the RF testing of the SAW device is shown in Figure 12. The SAW device was immersed in a Cryofab CMSH-30 thirty liter dewar of liquid helium. An American Magnetics helium level probe was used to

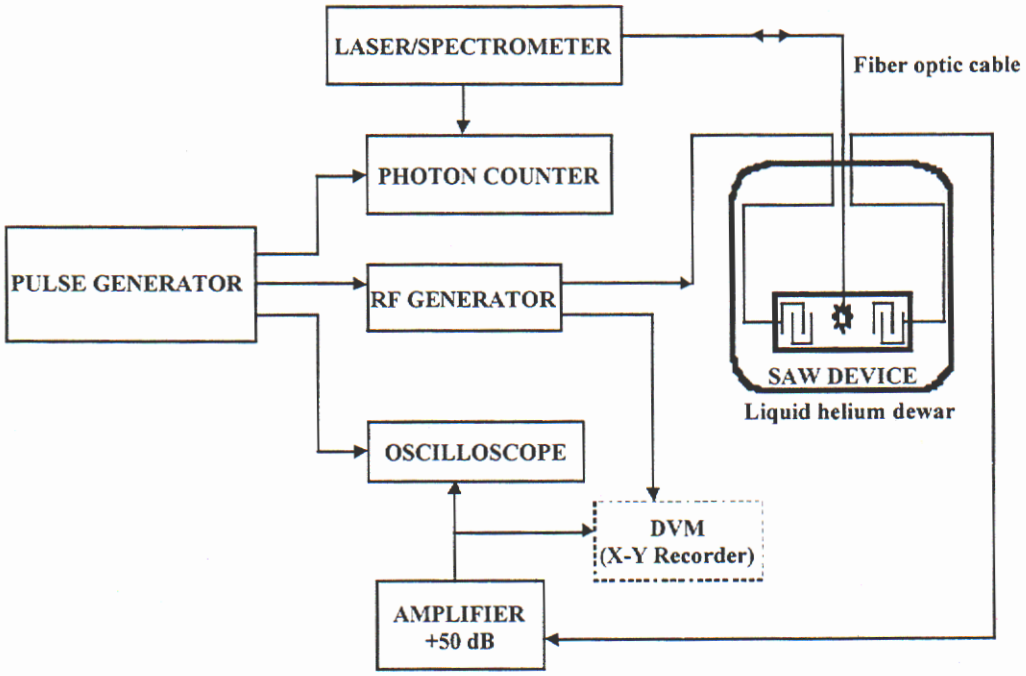

Figure 12: An overview of the RF test set-up

monitor the liquid helium level in the dewar. For the pulsed experiments, the Systron-Donner Model 101C pulse generator was used to send a pulse to the HP8341B RF generator, the Tektronix Model 485 oscilloscope, and the Stanford SR400 photon counter. After receiving this pulse, the RF generator sends a voltage pulse to the SAW device to initiate the surface acoustic wave. The oscilloscope's external trigger was also set by the pulse generator's pulse to display the acoustic signal coming out the SAW device relative to the RF generator's pulse input. The pulse generator's pulse was also used to trigger the photon counter to begin the photon count when the surface acoustic wave was passing underneath the fiber. The HP8447B amplifier gives a 50 dB amplification of the SAW device output signal for display on the oscilloscope. The digital voltmeter (DVM) and x-y recorder were used in the CW mode when the initial frequency spectrum sweeps of the SAW devices were made. These were necessary to find the device attenuation versus frequency.

The photon counter measures the photoluminescence signal by counting the number of photons during a gated period. A first count is taken when the acoustic wave is passing underneath the fiber. A second count is taken when the acoustic wave has gone past the

fiber. The photon counter then takes the difference. This gives a direct indication of how many excitons have been transported. The gate delay for the second count period was set at 2.5 μsec. The center-to-center wave path between transducers is 2421 μm and the velocity of sound in gallium arsenide is 2865 m/sec, giving a time of approximately 0.85 μsec for the acoustic wave to traverse the wave path. The value of 2.5 μsec was used to assure that the surface acoustic wave had passed and would not affect the photon count. The optimal gate delay for the first photon count was found empirically by varying this gate delay from 150 to 1000 nsec and finding the time where the maximum difference between the first and second counts occurred, which is where the most excitons were being swept away. The repetition rate for the photon counting sequence was every 3μsec.

Signal discriminators are used to provide signal to noise improvement in the photon counter by blocking the low amplitude noise pulses from the photomultiplier tube. As the discriminator voltage level is increased, fewer photons have the necessary pulse height to be counted. The discriminator voltage level for the A-gated photon counter was chosen to be well above the noise level, and the value for the B-gated photon counter was adjusted to give a minimum in the differential photon count measurement with no applied RF excitation voltage. This adjustment was necessary due to the inherent variation between the two discriminators.

2.7 RF testing

The waveform timing diagram is shown in Figure 13. To initiate one differential photon count measurement, the pulse modulation output from the pulse generator would be sent. The pulse width was varied from 100 to 500 nsec in different experiments. After a delay due to the cable length (approximately 1 nsec/foot), the photon counter and gate delays are triggered. The RF output is triggered after a slightly longer delay due to a cable delay plus a built-in RF generator delay. This RF pulse is sent to the SAW device transmitter, initiating the surface acoustic wave. After the empirically determined optimal gate delay (shown here to be 575 nsec), the A-gated photon counter is started. The gate width for counting was manually set to be the same width as the pulse generator pulse width. The surface acoustic wave has been travelling across the substrate and it takes approximately 850 nsec to travel to the receiving transducer and initiate the surface acoustic wave

in this region. At time t = 2.5 μsec plus the initial photon counter cable delay, the B-gated photon counter is begun (this is not shown on the figure to avoid unnecessary elongation of the x-axis). At time t = 3 μsec, the sequence was started over.

2.8 Generation of excitons

Light from the argon-krypton laser (λ = 514.5 nm) was used for optical interband excitation above the GaAs quantum well bandgap energy. Laser illumination and detection were done at the same spot on the sample, approximately equidistant from both transducers. In the moving potential superlattice with wavelength λ = 14 μm, the excitons become polarized predominantly by the lateral electric field until they dissociate at high fields into spatially separated electron-hole pairs. The electrons and holes are then trapped in their respective energetic minima, i.e., the electrons in the potential minima of the SAW which are the regions of positive electric potential, and the holes in the valence band maxima which are the regions of negative electric potential[3] (see Figure 3). As the potential modulation is moving with the speed of sound, the spatially separated and trapped electron-hole pairs are swept away by the SAW and are propagated across the sample without recombining.

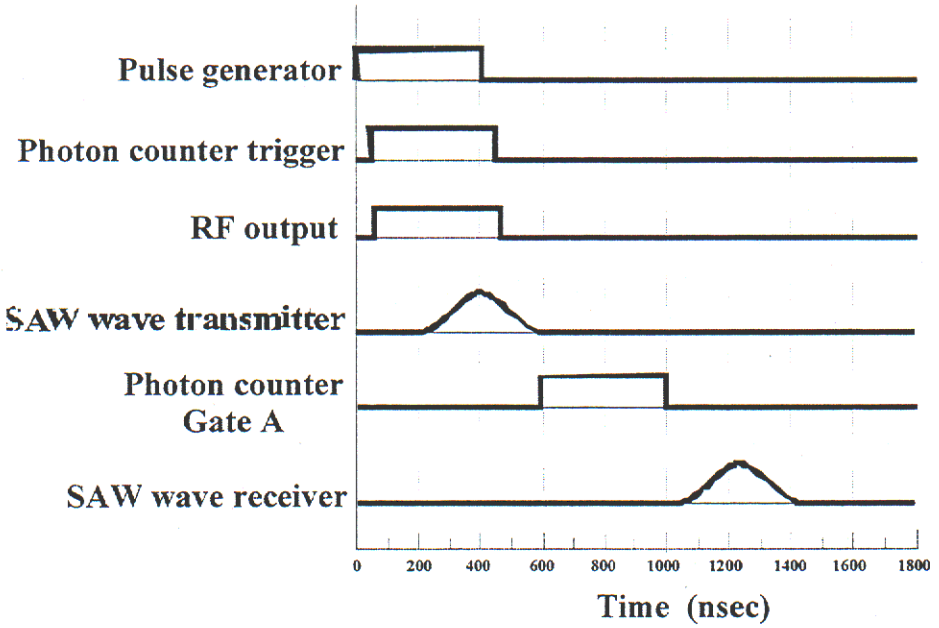

Figure 13: RF testing waveform timing diagram

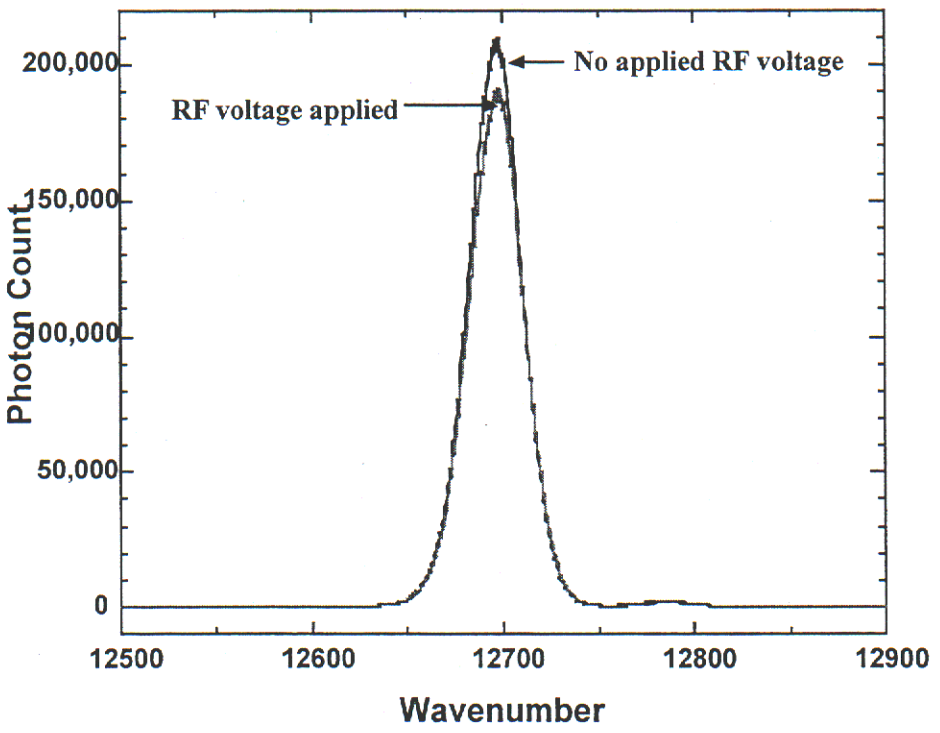

Figure 14: Two photoluminescence spectra for the GaAs/AlGaAs quantum well structure, with and without applied SAW RF voltage

3. Results and Discussion

3.1 Photoluminescence spectra

Several photoluminescence spectra were taken in areas around the wafer after it was grown to initially gauge photon counts versus wavenumber and check the purity of the gallium arsenide sample. Pure samples give a narrow wavenumber peak while impurities cause multiple or rounded peaks. These initial spectra showed the wafer to be of good quality, having a narrow line width, and hence, it looked promising for use in this experiment.

Before the RF testing was begun, another spectrum was taken to check the photoluminescence at the exact spot where the laser would hit the SAW device. Figure 14 shows the photoluminescence spectra for the two cases where the SAW device did and did not have an applied RF voltage. The photon count can be seen to decrease from approximately 210,000 with no applied RF voltage to 190,000 when an RF voltage was applied, while the exciton energy was constant at approximately 12699 cm^{-1}.

The photoluminescence spectra with and without the applied RF voltage shows the generation of excitons in the GaAs/AlGaAs quantum well structure designed for this research. This demonstrates the first of the three objectives for this work.

3.2 Network analysis of SAW device

The SAW devices were analyzed at room temperature using Cascade Microtech microprobes and a HP Model 8753 network analyzer. The insertion loss versus frequency curve for the 200 MHz SAW device is shown in Figure 15. The network analysis shows a frequency peak at approximately 198.6 MHz, which is very near the 200 MHz for which the IDTs were designed. The quality factor, B, as calculated by the center frequency divided by the change in frequency using Eq. 6, is found to be approximately 26.5. Theoretically for forty finger-pairs, this should be 20. The experimental bandwidth is found to be approximately 7.5 MHz; the theoretical value from Eq. 6 is 10 MHz. The typical lsin (x)/xl curve which is theoretically expected from the SAW device (see figure 6) can be seen to be altered. The distinct lobes of the sinc function have become muted. This mutation is due to triple transit reflection which is a situation where an initial acoustic wave is

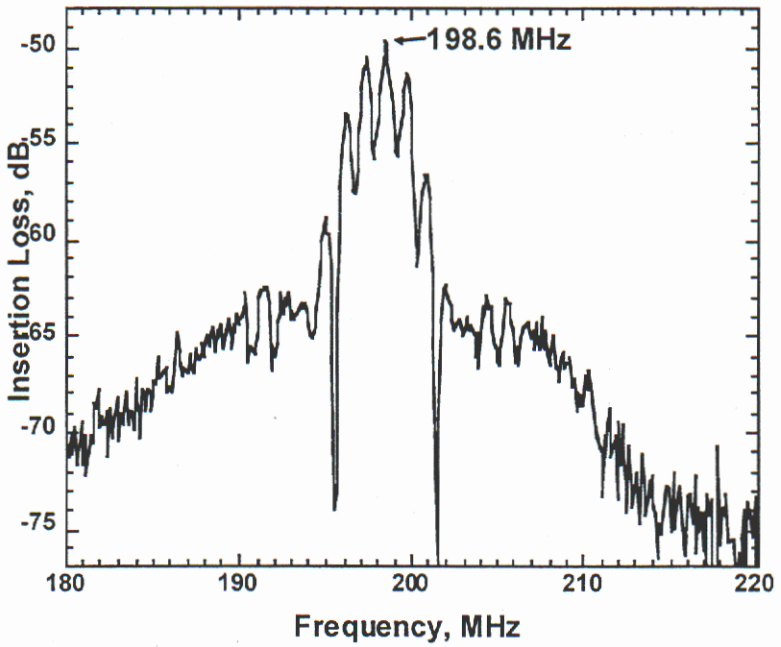

Figure 15: The SAW device network analysis curve, showing the peak frequency to be approximately 198.6 MHz, with a minimum insertion loss of –50 dB

launched by the transmitting IDT, reflected backwards from the receiving IDT, reflected back again from the transmitting IDT, then finally received by the receiving IDT. Triple transit reflection alters and attenuates the output signal. This situation can be due to too much IDT metal but it also can happen due to the waves reflecting off the smooth end of the substrate. When the devices fabricated for this experiment were diced, the edges were ragged which limited this cause for triple transit reflection. The edges of the etch underneath the transducers could be a source for the reflections. The main cause of the reflections, however, is most likely that too much IDT metal was deposited during the fabrication of the device. The 1650 Å of titanium and gold which were deposited on these devices act as a reflecting barrier, sending the incoming wave back into itself. However, the SAW device was considered to be usable for RF testing in that there still was approxi-

mately 13 dB of insertion loss between the usable frequency peak and the baseline acoustic signal.

The network analysis shows that the fabrication of the SAW devices on the GaAs/AlGaAs quantum well structure was accomplished and that the surface acoustic waves were generated successfully. This was the second of the three objectives for this study.

It should be noted that to bring about the transport of excitons using surface acoustic waves, only one transducer is actually necessary. If the wave is known to be launched successfully, a receiving transducer would be redundant since information on the surface acoustic wave is not necessary to know if excitons are moved. However, an objective of this report was to fabricate the SAW devices on the GaAs/AlGaAs quantum well structure and show that the surface acoustic waves could be generated. To do this entailed having a receiving transducer.

3.3 RF testing results

The RF testing of the SAW device was done at T = 4.2 K using the low temperature optical system configuration shown in Figure 12 to measure the photon output as a function of the applied electrical field (power) to the SAW device. The RF pulse width, and accordingly the channels A and B photon counter gate widths, were varied from 100 to 500 nsec in 100 nsec increments. For each value of pulse width, the applied peak-to-peak voltage was varied from approximately 0.3 to 3 volts. The differential photon count, which is the number of photons counted when the surface acoustic wave has passed minus the number when it is present, was monitored. This should be a positive value, since fewer photons should be counted when the surface acoustic wave is present. It was hypothesized that as the RF pulse width was increased, more ionized excitons would be swept away by the surface acoustic wave, and the differential photon count would become a larger positive value. Also, for increasing pulse width values, the slope of the differential photon count versus applied voltage should be larger. This is due to the fact that when the applied voltage is zero, the differential photon count should be zero for any pulse width curve, and at larger applied voltages, the differential photon count will be more positive for a longer pulse width. Figure 16 shows the differential photon counts versus applied peak-to-peak

voltage for RF pulse widths of 100, 200, 300, 400, and 500 nsec. As the pulse widths are increased, the differential photon count can be seen to increase, as expected. More ionized excitons are being swept away with the longer pulse. It can also be seen that the slope increases for increasing pulse widths, implying that at a given voltage, more ionized excitons are swept away with a longer pulse width. The standard deviation for ten differential photon count readings was calculated for each data point. A typical value is shown on the plot.

It should be noted that a y-offset has been added to the 500 nsec pulse width curve. The slope was obviously unaffected by this change; the offset was added to place the lowest voltage value in the 500 nsec pulse width curve higher on the y-axis than that of the corresponding point in the 400 nsec pulse width curve. The data shows the 500 nsec pulse

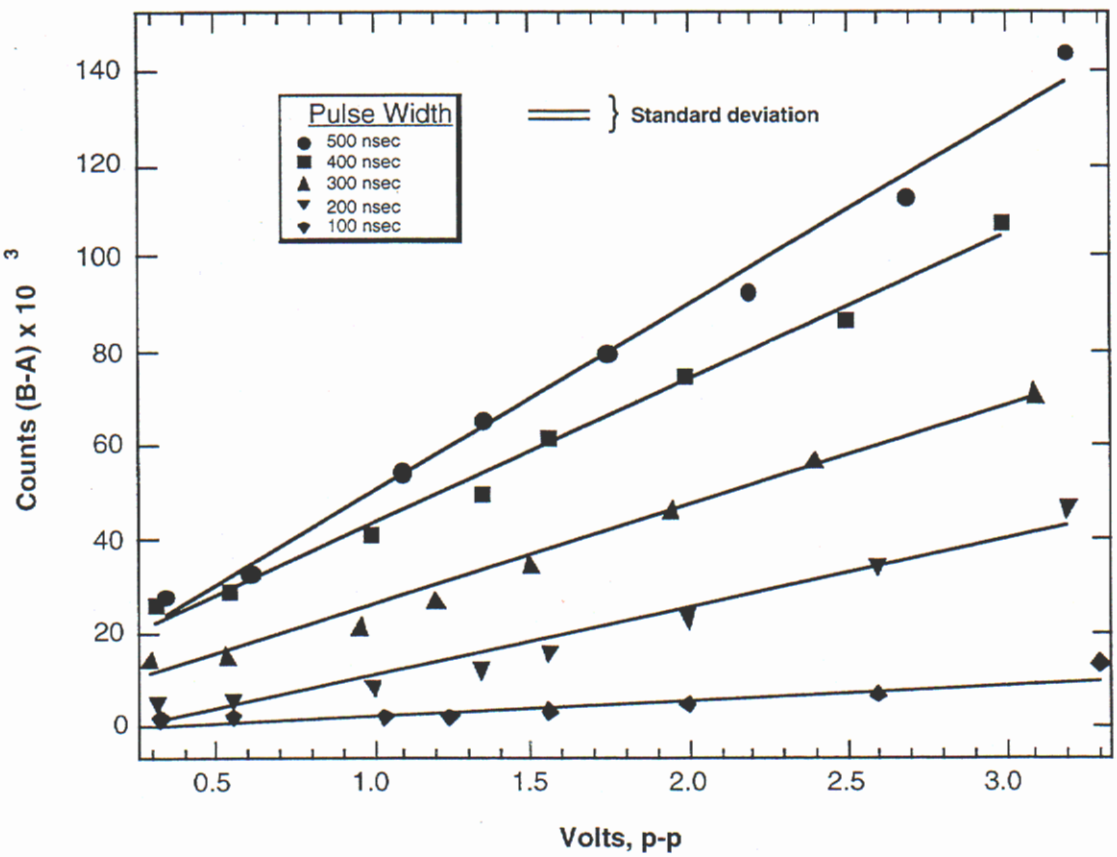

Figure 16: The differential photon count versus the applied peak-to-peak RF voltage for pulse widths of 100 to 500 nsec. Higher counts are seen for longer pulse widths and for larger applied voltages

width curve to have a negative differential photon count for peak-to-peak voltages below approximately one volt. This would correlate to a situation where more photons are counted when the surface acoustic wave is present than when it is gone, which is obviously an error. One possible explanation for this situation is that the discriminator voltage levels for the photon counter were not calibrated correctly for this run. Drift of these levels could introduce experimental error, where the differential photon count is no longer zero with no applied RF excitation voltage. The discriminator voltage levels for the five data sets were initially set to give a zero differential count for the 100 nsec data set and not rechecked during the subsequent testing with longer pulse widths. If the level for gate B would drift upward, giving a lower photon count, while the level for gate A would drift downward, giving a higher photon count, the differential (B-A) photon count could then go negative. This is the most likely cause for the anomalous negative differential photon count seen in the 500 nsec pulse width data set.

A discussion of the y-intercepts of each of the curves in Figure 16 needs to be covered. In the voltage range used for these data sets, 0.3 to 3 volts, the differential photon count can be approximated as linear, as is shown by the linear least squares fit attached to each data set. Extrapolating this linearity to zero volts, however, does not show a zero photon count, as would be expected. This is due to the fact that below 0.3 volts, these data sets are not linear. Previous testing showed that below this point, the differential photon count versus pulse width is essentially parabolic to zero. Below a certain applied turn-on voltage, the surface acoustic waves do not transport excitons efficiently. The data sets used for this research were focused on the region where the data sets were essentially linear. Therefore, the y-intercepts of the linear fits do not show a value of zero for the differential photon count.

Each of the pulse width curves in Figure 16 has a linear least squares fit plotted with it. Figure 17 is a plot of the slope of each of these fits versus pulse width. The slope, which is differential counts per peak-to-peak volt, can be seen to increase with pulse width. This

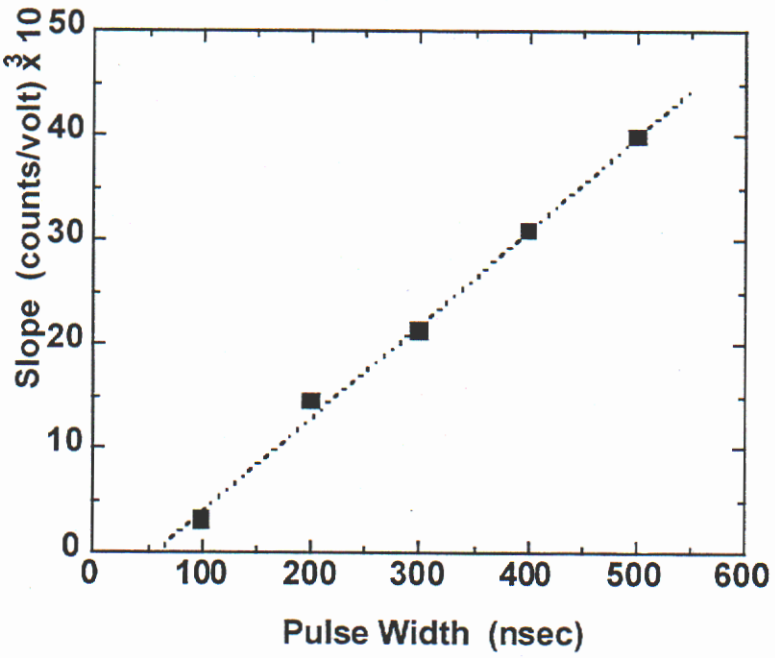

Figure 17: The slope of each of the curves in Figure 16 is plotted versus pulse width, showing that the number of excitons transported is directly proportional to pulse width.

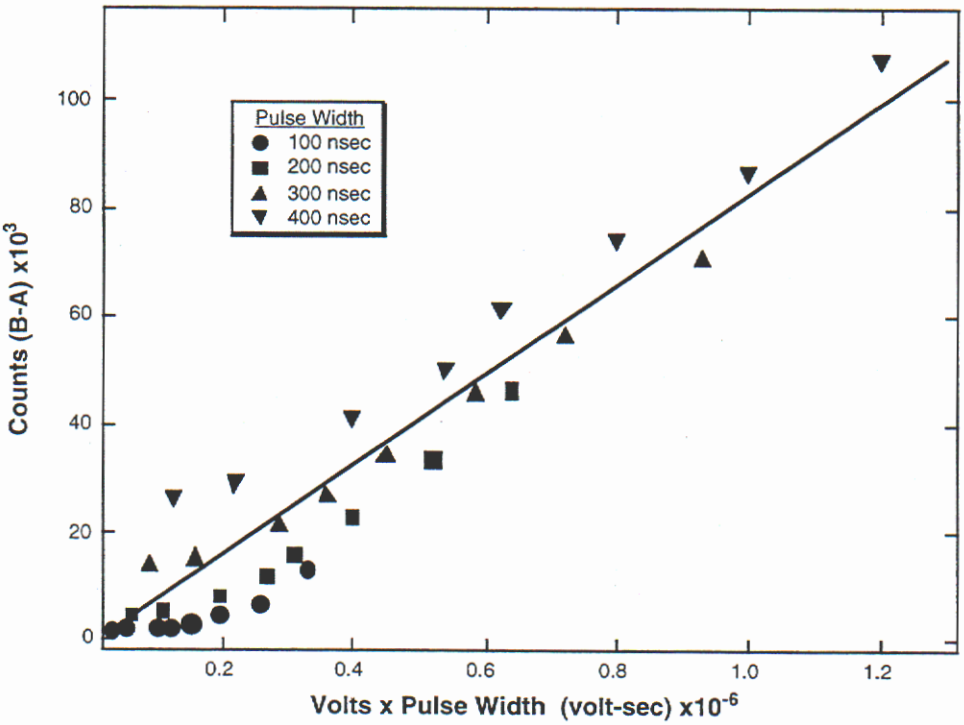

Figure 18: This comprehensive plot shows the differential photon count versus the normalized term of peak-to-peak RF voltage multiplied by the pulse width

is a clear indication that the number of excitons transported is directly proportional to pulse width: more excitons are transported with longer pulse widths.

Figure 18 shows the differential photon count versus the experimental data normalized on the x-axis by multiplying the peak-to-peak voltage by the pulse width for each of the pulse width curves, 100 to 400 nsec. The 500 nsec pulse width data set was excluded from this plot, because of the arbitrary y-offset necessary to place this plot higher on the y-axis than the 400 nsec data set. When plotted this way, it can be seen that the slope of each of the pulse width curves is approximately the same, while the differential photon count increases for longer pulse widths. The conglomerate view given in the figure shows that the differential photon count was monotonically increasing when voltage and pulse width were normalized.

The third objective of this study has now been shown. Figures 16-18 have shown the interaction of excitons and surface acoustic waves under varying pulse width and applied voltage conditions. It can be seen that surface acoustic waves can transport laser-generated excitons using a GaAs/AlGaAs quantum well structure.

4. Conclusions and Future Directions

4.1 Conclusions

This experiment has demonstrated that excitons can be transported in GaAs/AlGaAs quantum wells using surface acoustic waves. As the pulse width and applied RF voltage was increased, the differential photon count became more positive, indicating the movement of the excitons.

This report has described the quantum well and surface acoustic wave device design necessary to verify the original hypothesis. The photoluminescence spectra demonstrated that excitons could be generated in the GaAs/AlGaAs quantum well structure. Sample fabrication was detailed along with the necessary instrumentation to implement the cryogenic testing. The network analysis showed the fabricated SAW device characterization to be adequate for use in this research. Finally, the details and results of the SAW device RF testing were given to fully document the steps involved in demonstrating that this research topic was successful.

4.2 Exciton transport versus fewer excitons

There are two questions which need to be discussed regarding the justification of exciton transport. How does one justify that excitons were actually being swept away and not merely that fewer excitons were present when the surface acoustic wave was initiated? Also, could the excitons have collapsed, recombined, and possibly been converted into lattice vibrations (phonons)? These questions deserve some attention.

Could fewer excitons have been present when the surface acoustic wave was initiated? The number of excitons is dependent on the number of photons absorbed by the semiconductor. When a photon is absorbed in a direct bandgap semiconductor, an exciton is generated in the illuminated region. If there are no interactions that perturb the exciton, it will emit a photon in the same location where the exciton was generated, with an energy equal to the semiconductor bandgap energy minus the binding energy of the exciton. The presence of a surface acoustic wave affects the location where the exciton recombines, causing it to recombine at a remote location, but it does not affect the number of excitons

generated. The same number of excitons is present whether or not there is an applied RF voltage to the SAW device.

Could the excitons have collapsed, recombined, and been converted into phonons? A phonon is a quantum particle associated with the lattice vibrations of a crystal. Excitons can be converted into phonons, but in this situation, the probability of this happening is low. The bandgap energy of gallium arsenide at 4 K is about 1510 meV, while the maximum energy emitted per longitudinal optical (LO) phonon in gallium arsenide is 37 meV.[13] The LO phonon is the principle phonon energy in gallium arsenide. By conservation of energy, approximately 41 phonons would have to be simultaneously emitted for each exciton. The probability of this happening would be very small; first order processes dominate over higher order processes.[14] It would be much more likely to emit one photon than 41 phonons at any one time. Experimental data has shown that if an oscillator strength of value 1.0 is assigned to the exciton, the phonon could be assigned a maximum relative strength of 0.1. The probability of emitting 41 simultaneous phonons would then be $(0.1)^{41}$, which would be extremely low. This assumes no other simultaneous processes due to impurities. For the sample used for this research, however, the ultrapure sample quality has been demonstrated by the photoluminescence spectra of Figure 14, showing a photon count of approximately 200,000 taken at a power density of 1 $\mu W/cm^2$ with no phonon sidebands or background impurity effects. The high count rate at such a low power density shows the sample to be optically pure. Therefore, due to the facts that the sample used was ultrapure in quality and that there was no evidence of sidebands on the photoluminescence spectra, it can safely be assumed that very few of the excitons were converted to phonons.

4.3 Design problems

Concerning the three objectives of this research, the generation of excitons and the investigation of the interaction of the excitons and surface acoustic waves worked suffi-

ciently well to achieve the objectives of this study. The SAW device, while functional for this experiment, could be optimized.

One major concern with the surface acoustic wave device design was the use of too much metal, which caused triple transit reflection problems. For exciton transport, triple transit reflections pose the problem of determining the timing of the surface acoustic wave and being able to evaluate where the exciton is being transported. Further research could be undertaken to minimize the amount of metal while maximizing the acoustic signal. There would be a lower limit as to how thin the metal could be before the acoustic signal degrades. Future research could investigate gold metallization in the 500 – 1000 Å range. As discussed in Section 3.2, however, two transducers are not necessary for exciton transport. If future research does not require the SAW device characterization as well as the exciton transport information, the receiving transducer could be eliminated and this cause of triple transit reflection would be moot.

The other triple transit reflection concern was the reflection of the surface acoustic wave off the edge of the etch. Future research could be geared toward a wet etching process. Dry etching, such as the reactive-ion etching used for this research, leaves a straight-wall profile. Wet etching could roughen the edges and make the reflective angle something other than 180 degrees. This would allow the etch edge to reflect at an angle that is not directly back into the oncoming wave.

The bandwidth of the surface acoustic wave signal was adequate for this experiment, but it could be made narrower by incorporating more finger-pairs into the IDTs. A narrow bandwidth is desirable to avoid spurious oscillations and to improve the frequency stability of the device. A future modification for this design would be to increase the number of finger-pairs to fifty to narrow the bandwidth. This should also increase the insertion loss difference between the usable frequency peak and the baseline acoustic signal.

Another issue that warrants some attention is the fact that the network analysis of these SAW devices (see figure 15) showed a minimum insertion loss to be at approximately –50 dB. As insertion loss becomes more negative, more electrical energy is con-

verted to heat instead of piezoelectric energy. This experiment was done at liquid helium temperature, and adding heat to the system is not an optimal situation. Also, a stronger surface acoustic wave signal could transport more excitons. While this design for the SAW devices worked well enough to be used for this research, optimization of the SAW device design to give a less negative minimum insertion loss could be undertaken.

The design problems discussed in this section entailed the optimization of the SAW device. While the suggestions discussed are valid, the transport of excitons did not require an optimal surface acoustic wave. SAW device design modifications may, however, increase the number of excitons transported.

4.4 Future directions

Demonstrating that surface acoustic waves can be used to allow excitons to travel to other locations opens up many possibilities. The next step in this research could be to investigate a two-fiber setup to be able to locate where the exciton will recombine and give off the photon. Metallized stripes as well as etched grooves have been investigated to reflect an incoming surface acoustic wave to a predetermined location.[15] The use of a second acoustic wave propagating in the opposite direction to the initial wave has also been studied. If the amplitudes and frequencies of both waves are the same, a standing wave pattern is formed, and the electron-hole pairs recombine.[6] These may indicate a direction to take in solving how to bring about the exciton recombination at a specific location. A future direction could be to use the surface acoustic wave devices to build a photon racetrack, of sorts, in which four SAW devices are positioned at 90° to each other and are used to turn the transported exciton at right angles, eventually returning it to its original location. See Figure 19. The timing of this configuration would be such that the moving electron-hole pair would be almost ready to stop and recombine to emit a photon when the next surface acoustic wave would hit, redirecting it and send it travelling along into the next SAW device wave path. After a predetermined number of revolutions around the racetrack, the electron-hole pair would be kicked out of the loop by a fifth SAW device. This could lead to an application of this technology as a cipher lock or a variable optical delay

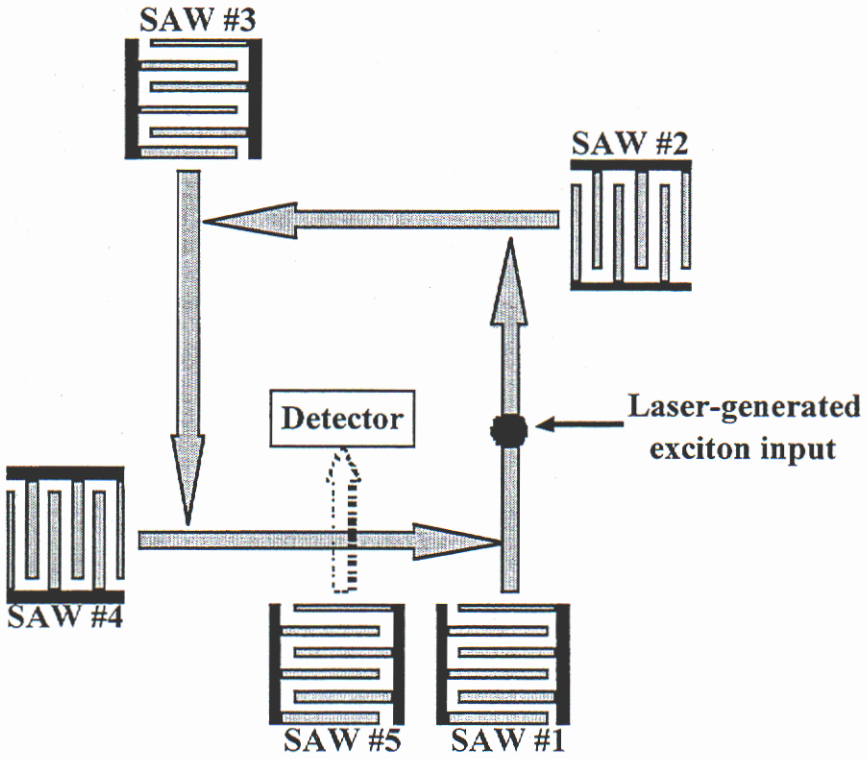

Figure 19: The photon racetrack, consisting of four SAW devices whose acoustic wave paths are at 90° to each other. The laser-generated exciton could be transported around the racetrack until the fifth SAW device is initiated to end the sequence.

line where the timing delay between the input and output positions is controlled by the timing sequence.

Real-world uses of this technology require operation of these devices at room temperature instead of at liquid helium temperature. Surface acoustic wave operation at room temperature is not a problem, but exciton generation is very temperature dependent. Temperature effects are a possibility for future investigation to ascertain if a room-temperature system for exciton transport would be viable.

4.5 Summary

The purpose of this study was to implement the instrumentation and fabricate the SAW devices to demonstrate the movement of excitons in a GaAs/AlGaAs quantum well using surface acoustic waves, in an effort to reproduce the previous work on this topic. The three objectives of this research were met: (1) the generation of excitons in the GaAs/AlGaAs quantum well structure was shown; (2) the fabrication of the SAW devices on the

GaAs/AlGaAs quantum well structure was achieved, and surface acoustic waves were generated; and (3) the interaction of the excitons and surface acoustic waves was investigated. The experimental methods, sample design and fabrication, and cryogenic testing were detailed to verify the steps involved in this experiment. The data has shown a more positive differential photon count when surface acoustic waves are present, indicating the movement of excitons by the surface acoustic waves. Longer pulse widths and larger applied RF voltages correlated with an increasingly more positive differential photon count, indicating more excitons being transported. Future directions in acousto-optic devices have been proposed.

References

1. A. Wixforth, J. Scriba, M. Wassermeier, J.P. Kotthaus, G. Weimann, and W. Schlapp, Phys. Rev. **B40**, 7874 (1989).
2. M.J. Hoskins, H. Morkoc, and B.J. Hunsinger, Appl. Phys. Lett. **41**, 332 (1982).
3. C. Rocke, S. Zimmerman, A. Wixforth, and J.P. Kotthaus, Phys. Rev. Lett. **78**, 4099 (1997).
4. C. Rocke, A.O. Govorov, and A.Wixforth, Phys. Rev. **B57**, R6850 (1998).
5. A. Wixforth, C. Rocke, S. Zimmerman, J.P. Kotthaus, G. Bohm, and G. Weimann, Physica **E 2**, 431 (1998).
6. A. Wixforth, Physica **E 3**, 145 (1998).
7. R.M. White, Proc. IEEE **58**, 1238 (1970).
8. E.A. Ash and E.G.S. Paige, editors, *Rayleigh-Wave Theory and Application* (Springer-Verlag, Berlin, 1985).
9. D.L. Dexter and R.S. Knox, *Excitons* (John Wiley & Sons, New York, 1965).
10. C.G. Kuper and G.D. Whitfield, editors, *Polarons and Excitons* (Oliver & Boyd, Ltd., Edinburgh, 1963).
11. S. Datta, *Surface Acoustic Wave Devices* (Prentice-Hall, Englewood Cliffs, NJ, 1986).
12. D.S. Ballantine, R. M. White, S. J. Martin, A. J. Ricco, E. T. Zellers, G. C. Frye, and H. Wohltjen, *Acoustic Wave Sensors: Theory, Design, and Physico-Chemical Applications* (Academic Press, San Diego, CA, 1997).
13. S. Blakemore, editor, *Gallium Arsenide* (American Institute of Physics, Long Island, NY, 1987).
14. K.F. Brennan, *The Physics of Semiconductors with Applications to Optoelectronic Devices* (Cambridge University Press, Cambridge, UK, 1999).
15. T.P. Cameron and W.D. Hunt, J. Appl. Phys. **84**, 2212 (1998).

Distribution:

1	MS-9018	Central Technical Files, 8945-1
2	MS-0899	Technical Library, 9616
1	MS-0612	Review and Approval Desk, 9612 for DOE/OSTI
1	MS-0161	Patent & Licensing Office, 11500
1	MS-0188	LDRD Office
10	MS-0601	E.D. Jones, 1123
1	MS-1764	S.J. Martin, 1764
1	MS-0537	P.A. Molley, 2331
1	MS-1427	J.M.Phillips, 1100
10	MS-0601	J. L. Reno, 1123
1	MS-1421	G. Samara, 1120
1	MS-0601	J. Simmons, 1123
10	MS-0537	B. L. Wampler, 2331
10	MS-0601	R.L. White, 1123
1	MS-1077	T.E. Zipperian, 1740